



HAL
open science

Dual-wavelength-pumping of mid-infrared Tm:YLF laser at 2.3 μm : demonstration of pump seeding and recycling processes

Hippolyte Dupont, Lauren Guillemot, Pavel Loiko, Alain Braud, Jean-Louis Doualan, Patrice Camy, Patrick Georges, Frédéric Druon

► To cite this version:

Hippolyte Dupont, Lauren Guillemot, Pavel Loiko, Alain Braud, Jean-Louis Doualan, et al.. Dual-wavelength-pumping of mid-infrared Tm:YLF laser at 2.3 μm : demonstration of pump seeding and recycling processes. *Optics Express*, 2022, 30 (18), pp.32141. 10.1364/OE.468695 . hal-03798899

HAL Id: hal-03798899

<https://hal-iogs.archives-ouvertes.fr/hal-03798899>

Submitted on 5 Oct 2022

HAL is a multi-disciplinary open access archive for the deposit and dissemination of scientific research documents, whether they are published or not. The documents may come from teaching and research institutions in France or abroad, or from public or private research centers.

L'archive ouverte pluridisciplinaire **HAL**, est destinée au dépôt et à la diffusion de documents scientifiques de niveau recherche, publiés ou non, émanant des établissements d'enseignement et de recherche français ou étrangers, des laboratoires publics ou privés.

Dual-wavelength-pumping of mid-infrared Tm:YLF laser at 2.3 μm : demonstration of pump seeding and recycling processes

HIPPOLYTE DUPONT,¹ LAUREN GUILLEMOT,² PAVEL LOIKO,² ALAIN BRAUD,² JEAN-LOUIS DOULAN,² PATRICE CAMY,² PATRICK GEORGES,¹ AND FRÉDÉRIC DRUON^{1,*}

¹Université Paris-Saclay, Institut d'Optique Graduate School, CNRS, Laboratoire Charles Fabry, 91127 Palaiseau, France

²Centre de Recherche sur les Ions, les Matériaux et la Photonique (CIMAP), UMR 6252 CEA-CNRS-ENSICAEN, Université de Caen, 6 Boulevard Maréchal Juin, 14050 Caen Cedex 4, France

*frederic.druon@institutoptique.fr

Abstract: Upconversion pumping of thulium lasers emitting around 2.3 μm (the $^3\text{H}_4 \rightarrow ^3\text{H}_5$ transition) has recently attracted a lot of attention as it is compatible with the mature Yb-laser technology. To explore this possibility, we built a mid-infrared Tm:LiYF₄ laser pumped by an Yb:CaF₂ laser at 1.05 μm delivering an output power of 110 mW at 2.31 μm for a maximum incident pump power of 2.0 W. A strong absorption issue appeared in the Tm laser: the slope efficiency vs. the incident pump power was 7.6% while that vs. the absorbed pump power reached 29%. To overcome this issue, a dual-wavelength pumping at 0.78 μm and 1.05 μm was explored (combining both the direct and upconversion pumping schemes). The reciprocal interplay between the two pumps was studied to evaluate their benefits in terms of the pump absorption and laser efficiency. We observed an interesting decrease of the laser threshold for upconversion pumping when adding a small fraction of the direct pump revealing a seeding effect for the excited-state absorption from the metastable $^3\text{F}_4$ level. A recycling process of this manifold by excited-state absorption in the $^3\text{F}_4 \rightarrow ^3\text{F}_{2,3}$ loop was also observed. The pump absorption seeding is a viable route for the development of low-threshold upconversion pumped thulium lasers.

© 2022 Optical Society of America under the terms of the [OSA Open Access Publishing Agreement](#)

1. Introduction

Mid-infrared (MIR) lasers emitting at the wavelengths around 2.3 μm (falling into the 2.0–2.4 μm atmospheric window, the K band) are of practical importance for spectroscopy of various atmospheric and biological species such as HF, CO, CH₄, H₂CO and C₆H₁₂O₆ leading to applications in the atmosphere gas sensing and pollutant detection, combustion studies and non-invasive glucose blood measurements [1,2]. Such laser sources are also interesting for pumping of mid-infrared optical parametric oscillators (OPOs) [3].

There exist several approaches to address this spectral range, namely by using lasers based on zinc chalcogenide crystals (ZnS, ZnSe) doped with Cr²⁺ ions [4]; semiconductor (GaInAs / InP or GaInAsSb / GaSb) Vertical-Cavity Surface-Emitting Lasers (VCSELs) [5]; Raman-shifted pulsed Tm or Ho lasers with a fundamental emission at 2 μm [6] or (iv) OPOs [3]. Finally, the thulium ions (Tm³⁺) themselves can provide a direct generation of the 2.3 μm radiation [7,8] according to the $^3\text{H}_4 \rightarrow ^3\text{H}_5$ electronic transition, Fig. 1(a). Note that Tm³⁺ ions can be efficiently pumped at 0.78-0.8 μm (directly to the $^3\text{H}_4$ state) using commercial high-power AlGaAs laser diodes [9]. The main advantages of 2.3 μm bulk Tm lasers are the developed growth technology of high optical quality Tm³⁺-doped fluoride and oxide crystals, the availability of cheap ; simple and high-power pump sources (e.g., fiber-coupled AlGaAs diode lasers and Yb fiber lasers, see below) ; direct laser emission at 2.2-2.4 μm avoiding any

46 frequency conversion steps ; the possibility to operate both in the continuous-wave and pulsed
47 regimes and high quality of the laser beam. In this way, Tm lasers operating on the ${}^3\text{H}_4 \rightarrow {}^3\text{H}_5$
48 transition may represent a simple and cheap alternative to Cr^{2+} -ion-based lasers at the expense
49 of much narrower gain bandwidth. The emission range of such Tm lasers is also filling the gap
50 between other direct emission of rare-earth-ions in the near-mid-IR, namely Ho^{3+} (${}^5\text{I}_7 \rightarrow {}^5\text{I}_8$,
51 $\sim 2.1 \mu\text{m}$) and Er^{3+} (${}^4\text{I}_{11/2} \rightarrow {}^4\text{I}_{13/2}$, $\sim 2.8 \mu\text{m}$).

52 During the last years, a great progress in developing continuous-wave (CW) [10-14] and
53 mode-locked (ML) [15,16] Tm lasers operating on the ${}^3\text{H}_4 \rightarrow {}^3\text{H}_5$ transition has been
54 demonstrated using various (both fluoride and oxide) laser crystals. Guillemot *et al.* reported
55 on a CW Tm:KY₃F₁₀ laser directly pumped at 0.78 μm and generating 0.84 W at 2.34 μm [12].
56 Loiko *et al.* showed that the slope efficiency of such a laser may exceed the Stokes limit owing
57 to the efficient energy-transfer upconversion (ETU) process for adjacent Tm³⁺ ions, ${}^3\text{F}_4 + {}^3\text{F}_4$
58 $\rightarrow {}^3\text{H}_6 + {}^3\text{H}_4$, Fig. 1(a), refilling the upper laser manifold [10]. Soulard *et al.* reported on a
59 SESAM ML Tm:LiYF₄ laser delivering 94 ps pulses at 2.31 μm [15]. Canbaz *et al.* achieved
60 femtosecond pulses (514 fs) from a similar laser using the Kerr-lens mode-locking technique
61 [16]. Note that both ML lasers were pumped by a Ti:Sapphire laser at 0.78 μm .

62 Later, alternative upconversion (UC) pumping schemes at 1 μm and 1.5 μm were proposed
63 for such lasers [17,18]. Among them, the first one is more attractive as it is compatible with the
64 mature Yb-bulk and Yb-fiber laser technologies. It is based on a weak (non-resonant) ground-
65 state absorption (GSA) corresponding to the short-wave vibronic sideband of the ${}^3\text{H}_6 \rightarrow {}^3\text{H}_5$
66 Tm³⁺ absorption band and a strong (resonant) excited-state absorption (ESA) from the
67 metastable Tm³⁺ state, ${}^3\text{F}_4 \rightarrow {}^3\text{F}_{2,3}$, Fig. 1(a). The population of the intermediate level ${}^3\text{F}_4$ is
68 mainly provided by the photon avalanche effect [19] relying on both the above-mentioned
69 resonant ESA channel and the well-known cross-relaxation (CR) process for Tm³⁺ ions, ${}^3\text{H}_4 +$
70 ${}^3\text{H}_6 \rightarrow {}^3\text{F}_4 + {}^3\text{F}_4$. Note that due to the non-resonant nature of the GSA transition, the population
71 of the ${}^3\text{F}_4$ state via the non-radiative path from the short-living ${}^3\text{H}_5$ state is almost negligible.
72 The photon avalanche process recycles the populations of Tm³⁺ multiplets in favor of the ${}^3\text{H}_4$,
73 and ${}^3\text{F}_4$ ones acting as the upper laser level and the “effective” ground-state, respectively.
74 Tyazhev *et al.* reported on a watt-level Tm fluoride fiber laser generating 1.24 W at 2.28 μm
75 with a slope efficiency of 37% based on a single-wavelength UC pumping at 1.05 μm using an
76 Yb-fiber laser [20].

77 So far, the main disadvantages of the UC pumping scheme for bulk MIR Tm lasers are the
78 limited pump absorption and relatively high laser threshold. This is explained by the need of
79 populating the intermediate ${}^3\text{F}_4$ Tm³⁺ state via the photon avalanche mechanism which becomes
80 efficient only at high pump intensities. It would be attractive to combine both pump schemes
81 (direct and UC pumping) to improve these performances. Wang *et al.* studied dual-wavelength
82 pumping at 0.79 and 1.47 μm : a diode-pumped Tm:LiYF₄ laser delivered 1.8 W at 2.31 μm for
83 a total incident pump power of 70 W [21]. Besides the low optical-to-optical efficiency of only
84 2.5%, the output power of the Tm laser saturated while increasing the pump power at 1.47 μm
85 and no lasing under single UC pumping was achieved. Thus, the potential of dual-wavelength
86 pumping was not clearly revealed.

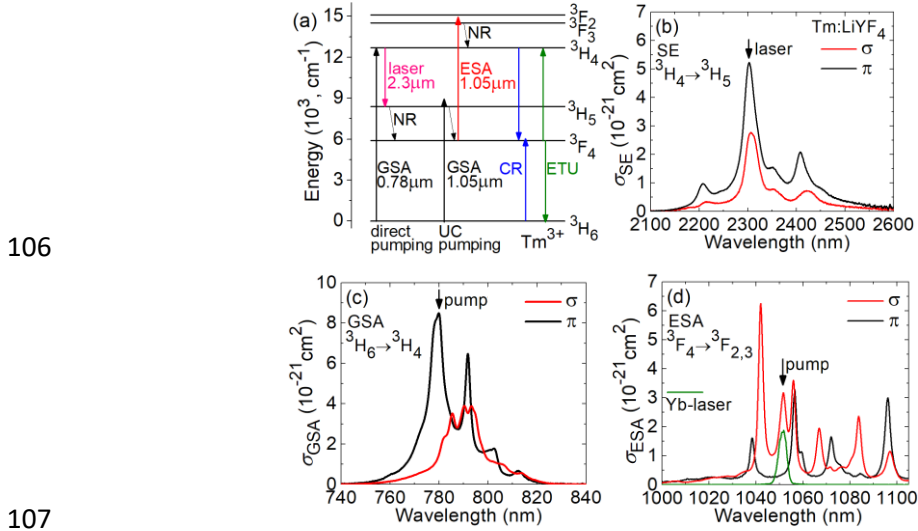
87 In the present work, we report on a mid-infrared thulium laser operating on the ${}^3\text{H}_4 \rightarrow {}^3\text{H}_5$
88 transition with a dual-wavelength (direct and upconversion) pumping at 0.78 and 1.05 μm (i.e.,
89 relying on the Yb-laser technology). As a gain material, we have selected Tm³⁺-doped lithium
90 yttrium fluoride crystal (LiYF₄) which currently appears as a state-of-the-art material for this
91 type of lasers.

92 2. Experimental

93 2.1 Spectroscopy of Tm:LiYF₄: An overview

94 Prior to the laser experiments, let us briefly describe the relevant spectroscopic parameters of
95 Tm³⁺ ions in the LiYF₄ crystal. The stimulated-emission cross-section for the ${}^3\text{H}_4 \rightarrow {}^3\text{H}_5$

96 transition reaches $\sigma_{SE} = 0.52 \times 10^{-20} \text{ cm}^2$ at 2303 nm for π -polarization, Fig. 1(b). The intrinsic
 97 lifetime of the upper laser level ${}^3\text{H}_4$ $\tau_{lum,0} = 2.3 \text{ ms}$ and for 3.5 at.% Tm doping, the self-
 98 quenching via CR leads to a reduced value of $\tau_{lum} \sim 155 \mu\text{s}$ [10]. For the ${}^3\text{H}_6 \rightarrow {}^3\text{H}_4$ GSA
 99 transition, the peak cross-section $\sigma_{GSA} = 0.85 \times 10^{-20} \text{ cm}^2$ at 779.9 nm for π -polarization
 100 (bandwidth at FWHM: 7.6 nm), see Fig. 1(c). For the ${}^3\text{F}_4 \rightarrow {}^3\text{F}_{2,3}$ ESA transition, the peak
 101 cross-section $\sigma_{ESA} = 0.63 \times 10^{-20} \text{ cm}^2$ at 1042.0 nm and at longer wavelengths, another less
 102 intense peak appears with $\sigma_{ESA} = 0.32 \times 10^{-20} \text{ cm}^2$ at 1051.6 nm (for σ -polarization), Fig. 1(d).
 103 The FWHMs of these peaks are 2.5 nm and 4.3 nm, respectively. The ${}^3\text{H}_6 \rightarrow {}^3\text{H}_5$ GSA is weak
 104 between 1000 nm and 1100nm ($\sigma_{GSA} \approx 0.01 \times 10^{-20} \text{ cm}^2$ in this region) since it is located in the
 105 tail of the peak at 1.20 μm (for π -polarization) that has a value of $\sigma_{ESA} = 0.62 \times 10^{-20} \text{ cm}^2$.



106
 107
 108 **Fig. 1.** (a) The scheme of energy levels of thulium ions relevant for MIR laser operation: GSA and ESA – ground- and excited-state absorption, respectively, NR – non-radiative relaxation,
 109 CR – cross-relaxation, ETU – energy-transfer upconversion; (b-d) Spectroscopy of Tm^{3+} ions in LiYF_4 : (b) simulated-emission (SE) cross-sections, σ_{SE} , the ${}^3\text{H}_4 \rightarrow {}^3\text{H}_5$ transition; (c) GSA cross-
 110 sections, σ_{GSA} , the ${}^3\text{H}_6 \rightarrow {}^3\text{H}_4$ transition; (d) ESA cross-sections, σ_{ESA} , the ${}^3\text{F}_4 \rightarrow {}^3\text{F}_{2,3}$ transition.
 111 The light polarizations: π and σ . In (d), the spectrum of the Yb:CaF₂ laser is shown for
 112 comparison.
 113
 114

115 2.2 Laser set-up

116 The scheme of the dual-wavelength-pumped MIR thulium laser is shown in Fig. 2. As a gain
 117 medium, we use an α -cut 3.5 at.% Tm:LiYF₄ crystal ($\Phi=8.5 \text{ mm}$, thickness=8.14 mm). Its faces
 118 are polished to laser-quality with good parallelism and left uncoated. The crystal is glued to a
 119 Cu-holder and it is passively cooled. A hemispherical laser cavity is composed of a flat pump
 120 mirror (PM) coated for high transmission (HT) at the pump wavelengths ($T = 95\%$ at 1.05 μm
 121 and 0.78 μm) and high reflection (HR, $R > 99.9\%$) at 2.3 μm , and a concave (radius of curvature:
 122 RoC = -100 mm) output coupler (OC) having a transmission at the laser wavelength $T_{OC} = 2\%$.
 123 The OC also provides HT at 1.9 μm to suppress the laser on the ${}^3\text{F}_4 \rightarrow {}^3\text{H}_6$ transition. The
 124 geometrical cavity length is 99 mm.

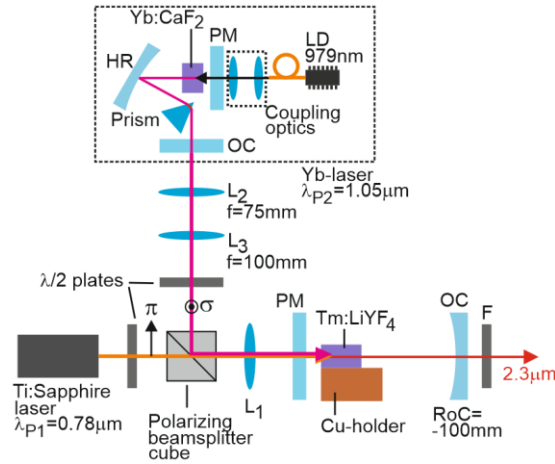


Fig. 2. Set-up of the dual-wavelength-pumped MIR thulium laser: PM – pump mirror, OC – output coupler, HR – highly-reflective mirror, L₁, L₂, L₃ – aspherical lenses, λ/2 – half-wave plates, LD – laser diode, F – band-pass filter.

125
126
127
128

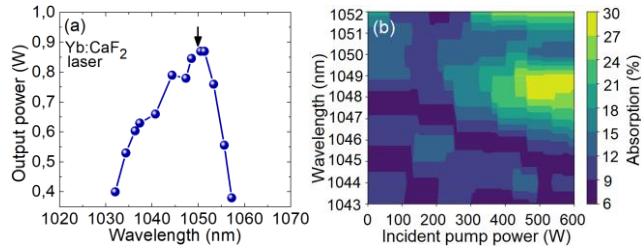
129 Two pump sources are used. The first one addresses the ${}^3\text{H}_6 \rightarrow {}^3\text{H}_4$ GSA transition (the
130 direct pumping). It is a Ti:Sapphire laser (Spectra Physics, model 3900J) delivering up to 3.0
131 W at $\lambda_{\text{P,GSA}} = 780$ nm (linewidth at FWHM: 0.1 nm) with a beam quality factor $M^2 \approx 1$ and a
132 linear polarization aligned to correspond to π in the Tm-crystal. Its output is focused into the
133 laser crystal using a lens (L₁). Several L₁ focusing lenses with a focal length in the range of 50
134 – 150 mm are tested. For $f = 150$ mm (the optimum one for single wavelength pumping at $\lambda_{\text{P,GSA}}$
135 = 0.78 μm), the measured pump beam waist $2w_{\text{P}}$ is 61 ± 5 μm .

136 The second pump source is designed to address the ${}^3\text{F}_4 \rightarrow {}^3\text{F}_{2,3}$ ESA transition (the UC
137 pumping scheme). A home-made tunable Ytterbium-bulk laser is based on a 2 at.% Yb:CaF₂
138 crystal pumped by a fiber-coupled InGaAs laser diode at 979 nm. A V-shaped laser cavity is
139 composed of a flat pump mirror, a concave (RoC = -200 mm) HR mirror and a plane OC (T_{OC}
140 = 5%). The wavelength tuning is realized by inserting an SF10 prism close to the OC. The
141 maximum of the output power of the tunable Yb:CaF₂ laser is observed at ~ 1.05 μm , thus, we
142 select the thulium ESA peak at 1051.6 nm for UC pumping, cf. Fig. 1(b), even though another
143 ESA peak at 1042.0 nm is more intense. The tunable Yb-laser delivers up to 1 W at $\lambda_{\text{P,UC}} =$
144 1050 nm (linewidth: ~ 3 nm) with a linear polarization corresponding to σ in the Tm-crystal.
145 Without the prism, in the free-running regime, the Yb-laser can be scaled up to 2 W (after the
146 polarizer Fig. 2) at a central wavelength of 1050 nm. The size of the pump beam from the Yb-
147 laser is adjusted using an afocal telescope system composed of two lenses (L₂: $f = 75$ mm, L₃:
148 $f = 100$ mm) and the polarization state – using a half-wave plate. For this pump source, the
149 measured pump spot size in the crystal $2w_{\text{P}}$ is 30 ± 5 μm (for L₁ lens with a focal length of $f =$
150 50 mm, being the optimum one for pure UC pumping). The two pump beams are combined
151 using a polarizing beam-splitter cube (Thorlabs PBS252). The pumping is in double-pass
152 because of the partial reflectivity of the OC at the pump wavelengths ($R_{0.78\mu\text{m}} = 64\%$ and $R_{1.05\mu\text{m}}$
153 = 28%). The residual (non-absorbed) pump after the OC is filtered out using a band-pass filter
154 (Thorlabs, FB2250-50).

155 3. Results and discussion

156 The wavelength of the Yb:CaF₂ laser is continuously tuned from 1032 to 1054 nm, Fig. 3(a).
157 To justify the selection of the pump wavelength, we have studied the single-pass pump
158 absorption as a function of $\lambda_{\text{P,UC}}$ and the incident pump power, Fig. 3(b). The highest pump
159 absorption is observed at 1050 nm in agreement with the ESA spectra of Tm³⁺ ions in LiYF₄
160 for σ -polarization, cf. Fig. 1(d). A certain pump level is needed to reach a kind of plateau for

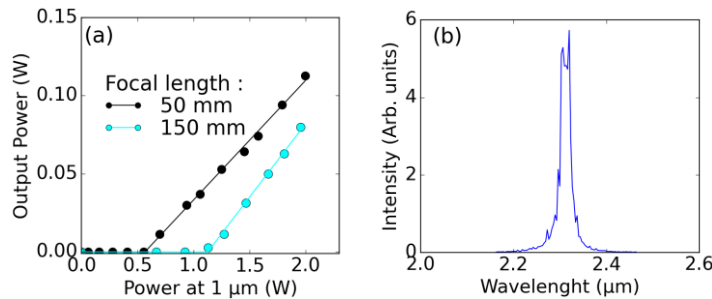
161 pump absorption (~30%). Thus, tuning the pump wavelength to match precisely one of the ESA
 162 peaks is indeed critical as otherwise we are not able to reach reasonably high pump absorption
 163 even for high pump levels.



164
 165 **Fig. 3.** (a) Wavelength tuning curve of the Yb:CaF₂ laser, *arrow* – the selected laser wavelength;
 166 (b) A 2D plot of single-pass pump absorption in the Tm:LiYF₄ crystal (σ-polarized pump) vs.
 167 the pump wavelength and the incident pump power.

168 Due to the different physical processes involved in the pump absorption between the cases
 169 of direct pumping (the GSA $^3H_6 \rightarrow ^3H_4$ transition following a classical Beer-Lambert absorption
 170 law) and UC pumping (the ESA $^3F_4 \rightarrow ^3F_{2,3}$ transition based on a photon avalanche effect), it
 171 is found that different focal lengths of the L₁ focusing lens lead to optimum laser performances
 172 in these two cases. Indeed, shorter focal length ($f = 50$ mm) is preferable for pure UC pumping
 173 as it leads to higher incident pump intensity and, thus, stronger photon avalanche effect and
 174 higher pump absorption. In contrast, for pure direct pumping, an L₁ lens with $f = 150$ mm
 175 provides better mode matching with a relatively good absorption efficiency since the absorption
 176 coefficient is independent of the pump intensity.

177 First, we study single-wavelength UC pumping. As explained above, an L₁ lens with a focal
 178 length of $f = 50$ mm is used, Fig. 4(a). Pumping at $\lambda_{p,UC} = 1.05$ μm (the $^3F_4 \rightarrow ^3F_{2,3}$ ESA
 179 transition), the output power of the MIR Tm-laser reaches 110 mW at 2.31 μm with a slope
 180 efficiency η of 7.6% (vs. the incident pump power $P_{1.05\mu m}$) and a laser threshold of 0.51 W.
 181 However, the slope efficiency vs. the absorbed pump power is relatively high, 29%, which then
 182 rises the interest of using the Yb-laser technology for pumping Tm³⁺-doped materials emitting
 183 at 2.3 μm. A typical spectrum of the laser emission is shown in Fig. 4(b). The laser emitted
 184 linearly polarized radiation (π) and its polarization state is naturally selected by the anisotropy
 185 of the gain medium. To illustrate the superiority of the short focal length L₁ lens for pure UC
 186 pumping, both the input-output dependences of the Tm-laser for $f = 50$ mm and $f = 150$ mm
 187 are given in Fig. 4(a). Using the latter lens, the maximum output power of the MIR Tm-laser
 188 was only 80 mW corresponding to an increased threshold of 1.2 W.
 189



190
 191 **Fig. 4.** Tm:LiYF₄ laser emitting at 2.3 μm with pure UC pumping by an Yb:CaF₂ laser emitting
 192 at 1050 nm: (a) input-output dependences for different focal lengths of the focusing lens (L₁): f
 193 = 50 mm and $f = 150$ mm; (b) a typical spectrum of laser emission.

194
 195 The dual-wavelength pumping is studied by fixing the power level of one pump source and

196 varying that of the second one. The laser output powers are plotted versus the total incident
 197 pump power, $P_{\Sigma} = P_{0.78\mu\text{m}} + P_{1.05\mu\text{m}}$ and the slope efficiency and the laser threshold are
 198 determined with respect to P_{Σ} – for fair comparison. To assist UC pumping, the $P_{0.78\mu\text{m}}$ value is
 199 fixed at several different levels and $P_{1.05\mu\text{m}}$ is varied, as shown in Fig. 5(a). With increasing the
 200 added $P_{0.78\mu\text{m}}$ power up to 2.0 W, both the maximum output power of the Tm-laser and its slope
 201 efficiency η gradually increase reaching 500 mW and 15.0%, respectively, Fig. 5(a,b).
 202

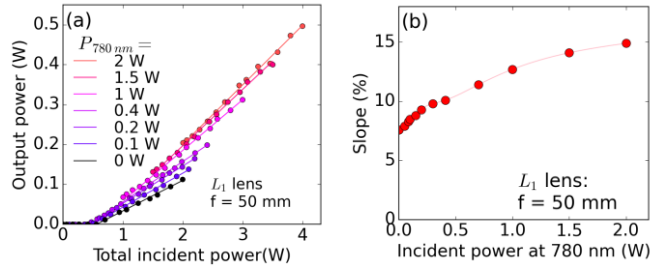


Fig. 5. Dual-wavelength-pumped MIR Tm:LiYF₄ laser, $P_{0.78\mu\text{m}}$ – fixed, $P_{1.05\mu\text{m}}$ – varied: (a) input-output dependences, L_1 focusing lens: $f = 50$ mm; (b) laser slope efficiencies vs. the total incident pump power (P_{Σ}) plotted against the added $P_{0.78\mu\text{m}}$ pump power

203

204

205

206

207 In all the experiments, the Tm-laser operates solely on the ${}^3\text{H}_4 \rightarrow {}^3\text{H}_5$ transition and no laser
 208 at $1.9\mu\text{m}$ is observed.

209

210 For completeness, we have also studied pure direct pumping using an L_1 lens with a focal
 211 length $f = 150$ mm. As the goal of the present work is the observation of the mutual interplay
 212 between the two pumps, the laser cavity and the pump focusing optics are not separately
 213 optimized for direct pumping as in the previous studies [10,11]. Pumping at $\lambda_{\text{P,GSA}} = 0.78\mu\text{m}$
 214 (the ${}^3\text{H}_6 \rightarrow {}^3\text{H}_4$ GSA transition), the MIR Tm-laser generates a maximum output power of 480
 215 mW at $2.31\mu\text{m}$ with a slope efficiency η of 20.9% (vs. the incident pump power $P_{0.78\mu\text{m}}$) and a
 216 laser threshold of 0.47 W, Fig. 6(a). Then, we have again implemented dual-wavelength
 217 pumping: the added $P_{1.05\mu\text{m}}$ pump power is fixed at different levels and $P_{0.78\mu\text{m}}$ varies, Fig. 6(a).
 218 With a maximum added $P_{1.05\mu\text{m}}$ pump power of 0.86 W, the maximum output power of the Tm-
 219 laser increases to 664 mW, its slope efficiency η increases to 24.5%, whilst the laser threshold
 220 also increases up to 0.85 W, Fig. 6(b). In this way, an addition of a small fraction of
 221 upconversion pump to the direct one has much weaker effect on the laser performance.

221

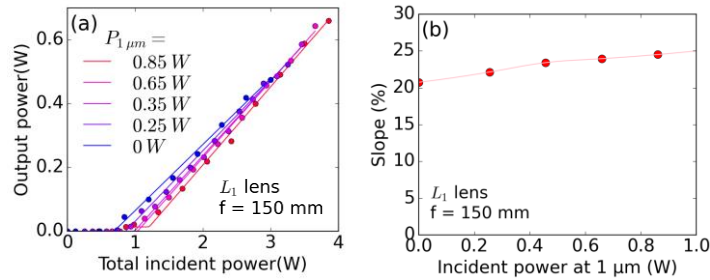


Fig. 6. Dual-wavelength-pumped MIR Tm:LiYF₄ laser: $P_{0.78\mu\text{m}}$ – varied, $P_{1.05\mu\text{m}}$ – fixed: (a) input-output dependences; (b) the corresponding laser slope efficiencies plotted against the added $P_{1.05\mu\text{m}}$ pump power. L_1 lens: $f = 150$ mm.

222

223

224

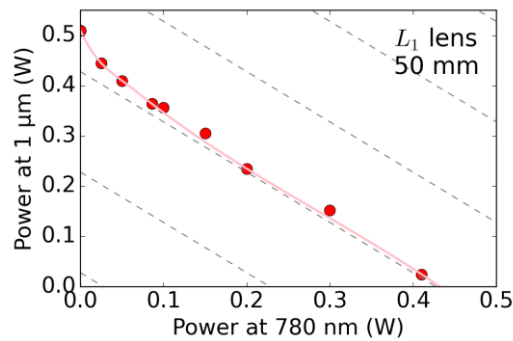
225

226 Let us discuss the observed laser behavior. The pumping at $0.78\mu\text{m}$ leads to a direct
 227 excitation of Tm³⁺ ions to the upper laser level (${}^3\text{F}_4$). It can result in an emission of a laser
 228 photon at $2.3\mu\text{m}$ followed by a non-radiative (NR) relaxation step to the intermediate

229 metastable level 3F_4 or in its population via the CR process for adjacent Tm^{3+} ions, ${}^3H_4 + {}^3H_6$
 230 $\rightarrow {}^3F_4 + {}^3F_4$. Thus, for direct pumping, the metastable 3F_4 Tm^{3+} state accumulates the electronic
 231 excitations. The UC pumping at $1.05\ \mu m$ is based on a weak (non-resonant) GSA, ${}^3H_6 \rightarrow {}^3H_5$,
 232 followed by a NR relaxation step to the 3F_4 state, and a resonant ESA, ${}^3F_4 \rightarrow {}^3F_{2,3}$, again
 233 followed by a NR relaxation step terminating at the upper laser level, 3H_4 . For low incident
 234 pump intensities, the ESA process is very weak because of the non-resonant GSA channel and,
 235 thus, negligible population of the metastable 3F_4 state. With increasing the incident pump
 236 intensity at $1.05\ \mu m$, both the 3H_4 and 3F_4 states accumulate electronic excitations owing to the
 237 photon avalanche mechanism based on a combination of the ESA and CR.

238 The population of the metastable 3F_4 state is crucial for boosting the efficiency of the ESA
 239 process ${}^3F_4 \rightarrow {}^3F_{2,3}$ which is a prerequisite for efficient laser operation under pure UC pumping
 240 and the population of this state could be easily increased by direct pumping representing a
 241 *seeding* effect on the UC pump absorption. It is indeed priming the UC pumping. Thus, dual-
 242 wavelength pumping relying mainly on the UC pump with a small addition of the direct pump
 243 could lead to reduced laser thresholds and boosted laser efficiencies of MIR Tm-lasers as
 244 compared to the case of pure UC pumping.

245 To illustrate this, we have plotted the measured laser thresholds of the dual-wavelength-
 246 pumped Tm laser for different combinations of the incident pump powers $P_{0.78\mu m}$ and $P_{1.05\mu m}$,
 247 Fig. 7. The L_1 lens with a focal length of 50 mm was chosen as it corresponded to the best
 248 performance in the case of pure UC pumping. In Fig. 7, each point represents a threshold pump
 249 power, $P_{th} = P_{0.78\mu m} + P_{1.05\mu m}$, then showing a combination of both pumps needed to reach the
 250 laser threshold. The intersections of this curve with the horizontal and vertical axes represent
 251 the two extreme cases of single-wavelength pumping: pure direct pumping with $\lambda_{p,GSA} = 0.78$
 252 μm on the abscise axis, and pure UC pumping with $\lambda_{p,UC} = 1.05\ \mu m$ on the ordinate axis,
 253 respectively. Compared to single-wavelength UC-pumping, an addition of even a small
 254 contribution of the direct pump ($P_{0.78\mu m} < 0.2\ W$) helps to notably reduce the laser threshold in
 255 terms of the total pump power. This is due to the seeding effect of the direct pump on the
 256 population of the intermediate 3F_4 state as explained above. To highlight this effect, we also
 257 plotted the isopower lines in order to clearly see that this process is more pronounced for a
 258 small fraction of the direct pump revealing then a seeding effect.

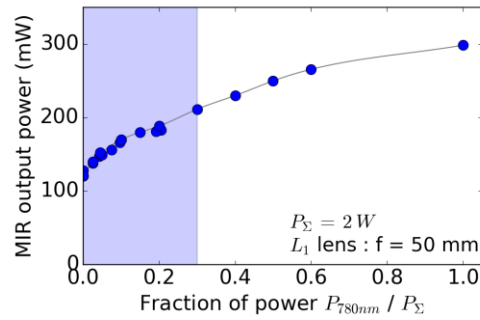


259
 260
 261
 262

Fig. 7. Analysis of the threshold behavior of the dual-wavelength pumped MIR Tm:LiYF₄ laser: thresholds for different combinations of the incident pump powers $P_{0.78\mu m}$ and $P_{1.05\mu m}$. Grey lines – isopower lines drawn as guides for eyes.

263 Another way to express the seeding effect of the added direct pump is to monitor the output
 264 power of the MIR Tm-laser as a function of the ratio between the added $P_{0.78\mu m}$ power and the
 265 total incident pump power P_{Σ} , namely $X = P_{0.78\mu m}/P_{\Sigma}$. Figure 8 illustrates such analysis for a
 266 fixed value of $P_{\Sigma} = 2.0\ W$ and for a focal length for L_1 of $f = 50\ mm$. Here, the cases of $X = 0$
 267 and $X = 1$ correspond to pure UC pumping and pure direct pumping, respectively. As can be
 268 seen from Fig. 8, the main effect of adding the direct pump on the output power is observed for
 269 small X values and for $X > 0.5$, the dependence saturates, therefore indicating an area of interest

270 towards lower X values.



271

272

273

274

Fig. 8. Output power of the dual-wavelength pumped MIR Tm:LiYF₄ laser as a function of the fraction of the direct pump to the total incident pump power, $P_{0.78\mu\text{m}}/P_{\Sigma}$. $P_{\Sigma} = 2.0$ W, L_1 lens: $f = 50$ mm. *Blue rectangle:* the zone of interest.

275

276

277

278

279

280

281

We have studied the total pump absorption in the Tm:LiYF₄ crystal at both wavelengths (0.78 μm and 1.05 μm) under single- and dual-wavelength pumping and non-lasing conditions, Fig. 9. To assist UC pumping, the added $P_{0.78\mu\text{m}}$ power is fixed at several different levels and $P_{1.05\mu\text{m}}$ varies. For this experiment, the focusing lens L_1 with a focal length of $f = 50$ mm is selected. One can then observe a strong effect of the dual-wavelength pumping on the pump absorption. This effect is also more impacting at lower level of $\lambda_{\text{P,GSA}} = 0.78$ μm

282

283

284

285

286

287

288

289

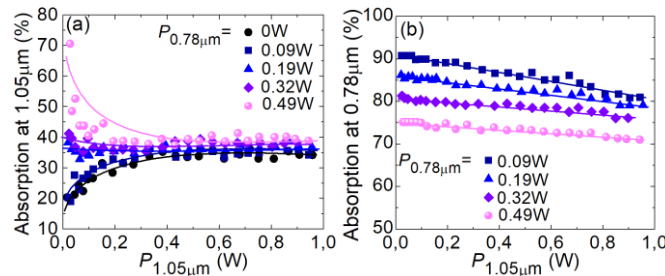
290

291

292

293

For pure UC pumping, Fig. 9(a), the pump absorption at 1.05 μm increases with the incident pump power and saturates at $\sim 34\%$ for $P_{1.05\mu\text{m}} > 0.4$ W. By adding more pump at 0.78 μm , this tendency changes first to almost pump-independent absorption (at $P_{0.78\mu\text{m}} = 0.19$ W) and then it is even reversed representing an absorption saturation effect. The saturated pump absorption slightly increases with the added $P_{0.78\mu\text{m}}$ power, from 34% to 40%, as shown in Fig. 9(a), representing a positive effect of the dual-wavelength pumping. These observations are in line with the laser behavior, and they are explained by the increased population of the metastable $^3\text{F}_4$ state acting as an “effective” ground-state for the $^3\text{F}_4 \rightarrow ^3\text{F}_{2,3}$ ESA channel. It is for the first time that we observe a *recycling* process of the population of the metastable $^3\text{F}_4$ state by ESA in the $^3\text{F}_4 \rightarrow ^3\text{F}_{2,3}$ loop favoring the 2.3 μm laser. Despite the fact that the measurements are performed under non-lasing conditions, as the main effect of the dual-wavelength pumping on the pump absorption is observed below the laser threshold, so that the obtained conclusions held true for the lasing regime as well.



294

295

296

297

Fig. 9. Total pump absorption for a dual-wavelength-pumped MIR Tm:LiYF₄ laser under non-lasing conditions measured at: (a) $\lambda_{\text{P,UC}} = 1.05$ μm , (b) $\lambda_{\text{P,GSA}} = 0.78$ μm , $P_{0.78\mu\text{m}}$ – fixed, $P_{1.05\mu\text{m}}$ – varied. L_1 lens, $f = 50$ mm.

298

299

300

301

A very different behavior is observed for the pump absorption at 0.78 μm . With increasing the pump power at 1.05 μm , it decreases marginally due to a slight decrease of the ground-state population since a part of the $^3\text{F}_4$ population is directly recycled in the upper loop instead of fluorescing back to the ground level. This recycling effect explains the increase of the laser

302 power and slope efficiency, Fig. 6(b), when using dual-pumping despite a lower absorption at
303 0.78 μm , cf. Fig. 9(b).

304 The observed rapid increase of the pump absorption at 1.05 μm under co-pumping at
305 0.78 μm (even for relatively low added pump powers) is responsible for the useful decrease of
306 the laser threshold of the dual-wavelength-pumped Tm:LiYF₄ laser, cf. Fig. 7. It is also partially
307 responsible of the increase of the laser slope efficiency, as shown in Fig. 5(b). Another possible
308 reason is the nonlinearity of the input-output dependences of Tm lasers operating on the $^3\text{H}_4 \rightarrow$
309 $^3\text{H}_5$ transition [12] due to the enhanced effect of ETU from the metastable $^3\text{F}_4$ state refilling the
310 upper laser level.

311 4. Conclusion

312 To conclude, we have studied in detail the dual-wavelength (combining direct and
313 upconversion) pumping of a Tm:LiYF₄ laser operating on the $^3\text{H}_4 \rightarrow ^3\text{H}_5$ transition
314 corresponding to an emission in the MIR, at 2.3 μm . As an UC pump source, we used a Yb:CaF₂
315 laser tuned to one of the ESA ($^3\text{F}_4 \rightarrow ^3\text{F}_{2,3}$) peaks of Tm³⁺ ions at 1.05 μm . Such fine matching
316 of the ESA peak was critical to reach a reasonably high pump absorption via the photon
317 avalanche mechanism. This particular matching between the Yb:CaF₂ pump and Tm:YLF laser
318 technologies was experimentally demonstrated for the first time, in our best knowledge. For
319 pure UC pumping, the MIR Tm laser delivered 110 mW at 2.31 μm for 2.0 W of incident pump
320 power corresponding to a slope efficiencies of 7.6% and 29% versus the incident and absorbed
321 pump power, respectively. Furthermore, we found that the co-pumping at 0.78 μm helps to
322 notably reduce the laser threshold due to the seeding effect on the population of the intermediate
323 $^3\text{F}_4$ Tm³⁺ state. We also observed a recycling process of this long-lifetime-manifold population
324 by resonant ESA that goes in favour of the 2.3 μm laser. Considering the availability of high-
325 power and high-brightness pump sources at 1 μm based on the Yb-fiber laser technology, and
326 low- to moderate-power single-mode fiber-coupled 0.8 μm AlGaAs laser diodes, a combination
327 of these two pump sources could serve as a viable way for the development of MIR Tm lasers,
328 especially those for which a high-brightness pumping and / or a compatibility with the fiber
329 laser technology are required, such as fiber and waveguide lasers and bulk femtosecond
330 oscillators and amplifiers. This is especially relevant for the latter type of laser sources which
331 are currently pumped by tunable Ti:Sapphire lasers thus strongly limiting their applications.

332 **Funding.** Agence Nationale de la Recherche (ANR-19-CE08-0028, SPLENDID2). “RELANCE” Chair of
333 Excellence project funded by the Normandy Region.

334 **Disclosures.** The authors declare no conflicts of interest.

335 **Data availability.** Data underlying the results presented in this paper are not publicly available at this time but may
336 be obtained from the authors upon reasonable request.

337 References

- 338 1. F. J. McAleavey, J. O’Gorman, J. F. Donegan, B. D. MacCraith, J. Hegarty and G. Maze, “Narrow linewidth,
339 tunable Tm³⁺-doped fluoride fiber laser for optical-based hydrocarbon gas sensing,” *IEEE J. Sel. Top. Quantum*
340 *Electron.* **3**(4), 1103-1111 (1997).
- 341 2. G. G. Taylor, D. Morozov, N. R. Gemmell, K. Erotokritou, S. Miki, H. Terai, and R. H. Hadfield, “Photon
342 counting LIDAR at 2.3 μm wavelength with superconducting nanowires,” *Opt. Express* **27**(26), 38147-38158
343 (2019).
- 344 3. V. Petrov, “Frequency down-conversion of solid-state laser sources to the mid-infrared spectral range using
345 non-oxide nonlinear crystals,” *Progr. Quantum Electron.* **42**, 1–106 (2015).
- 346 4. I. Moskalev, S. Mirov, M. Mirov, S. Vasilyev, V. Smolski, A. Zakrevskiy, and V. Gapontsev, “Ultrafast
347 middle-IR lasers and amplifiers based on polycrystalline Cr:ZnS and Cr:ZnSe,” *Opt. Mater. Express* **7**(7), 2636-
348 2650 (2017).
- 349 5. E. Geerlings, M. Rattunde, J. Schmitz, G. Kaufel, H. Zappe, and J. Wagner, “Widely tunable GaSb-based
350 external cavity diode laser emitting around 2.3 μm ,” *IEEE Photon. Technol. Lett.* **18**(18), 1913-1915 (2006).
- 351 6. U. Sheintop, D. Sebbag, P. Komm, S. Pearl, G. Marcus, and S. Noach, “Two-wavelength Tm:YLF/KGW
352 external-cavity Raman laser at 2197 nm and 2263 nm,” *Opt. Express* **27**(12), 17112-17121 (2019).

- 353
354
355
356
357
358
359
360
361
362
363
364
365
366
367
368
369
370
371
372
373
374
375
376
377
378
379
380
381
382
383
384
385
7. J. Caird, L. DeShazer, and J. Nella, "Characteristics of room-temperature 2.3- μm laser emission from Tm^{3+} in YAG and YAlO_3 ," *IEEE J. Quantum Electron.* **11**(11), 874-881 (1975).
 8. J. F. Pinto, L. Esterowitz, and G. H. Rosenblatt, " Tm^{3+} :YLF laser continuously tunable between 2.20 and 2.46 μm ," *Opt. Lett.* **19**(12), 883-885 (1994).
 9. E. Kifle, P. Loiko, L. Guillemot, J.-L. Doualan, F. Starecki, A. Braud, T. Georges, J. Rouvillain, and P. Camy, "Watt-level diode-pumped thulium lasers around 2.3 μm ," *Appl. Opt.* **59**(25), 7530-7539 (2020).
 10. P. Loiko, R. Soulard, L. Guillemot, G. Brasse, J.-L. Doualan, A. Braud, A. Tyazhev, A. Hideur, B. Guichardaz, F. Druon, and P. Camy, "Efficient $\text{Tm}:\text{LiYF}_4$ lasers at ~ 2.3 μm : Effect of energy-transfer upconversion," *IEEE J. Quantum Electron.* **55**(6), 1700212 (2019).
 11. I. Yorulmaz and A. Sennaroglu, "Low-threshold diode-pumped 2.3- μm Tm^{3+} :YLF lasers," *IEEE J. Sel. Top. Quantum Electron.* **24**(5), 1601007-1-7 (2018).
 12. L. Guillemot, P. Loiko, R. Soulard, A. Braud, J.-L. Doualan, A. Hideur, and P. Camy, "Close look on cubic $\text{Tm}:\text{KY}_3\text{F}_{10}$ crystal for highly efficient lasing on the ${}^3\text{H}_4 \rightarrow {}^3\text{H}_5$ transition," *Opt. Express* **28**(3), 3451-3463 (2020).
 13. P. Loiko, E. Kifle, L. Guillemot, J.-L. Doualan, F. Starecki, A. Braud, M. Aguiló, F. Díaz, V. Petrov, X. Mateos, and P. Camy, "Highly efficient 2.3 μm thulium lasers based on a high-phonon-energy crystal: evidence of vibronic-assisted emissions," *J. Opt. Soc. Am. B* **38**(2), 482-495 (2021).
 14. L. Guillemot, P. Loiko, A. Braud, J.-L. Doualan, A. Hideur, M. Koselja, R. Moncorge, and P. Camy, "Continuous-wave $\text{Tm}:\text{YAlO}_3$ laser at ~ 2.3 μm ," *Opt. Lett.* **44**(20), 5077-5080 (2019).
 15. R. Soulard, A. Tyazhev, J.L. Doualan, A. Braud, A. Hideur, M. Laroche, B. Xu, and P. Camy, "2.3 μm Tm^{3+} :YLF mode-locked laser," *Opt. Lett.* **42**(18), 3534-3536 (2017).
 16. F. Canbaz, I. Yorulmaz, and A. Sennaroglu, "Kerr-lens mode-locked 2.3- μm Tm^{3+} :YLF laser as a source of femtosecond pulses in the mid-infrared," *Opt. Lett.* **42**(19), 3964-3967 (2017).
 17. L. Guillemot, P. Loiko, R. Soulard, A. Braud, J.-L. Doualan, A. Hideur, R. Moncorgé, and P. Camy, "Thulium laser at ~ 2.3 μm based on upconversion pumping," *Opt. Lett.* **44**(16), 4071-4074 (2019).
 18. Y. Morova, M. Tonelli, V. Petrov, and A. Sennaroglu, "Upconversion pumping of a 2.3 μm $\text{Tm}^{3+}:\text{KY}_3\text{F}_{10}$ laser with a 1064 nm ytterbium fiber laser," *Opt. Lett.* **45**(4), 931-934 (2020).
 19. M. F. Joubert, S. Guy, and B. Jacquier, "Model of the photon-avalanche effect," *Phys. Rev. B* **48**(14), 10031-10037 (1993).
 20. A. Tyazhev, F. Starecki, S. Cozic, P. Loiko, L. Guillemot, A. Braud, F. Joulain, M. Tang, T. Godin, A. Hideur, and P. Camy, "Watt-level efficient 2.3 μm thulium fluoride fiber laser," *Opt. Lett.* **45**(20), 5788-5791 (2020).
 21. F. Wang, H. Huang, H. Chen, Y. Bao, Z. Li, and D. Shen, "GSA and ESA dual-wavelength pumped 2.3 μm $\text{Tm}:\text{YLF}$ laser on the ${}^3\text{H}_4 \rightarrow {}^3\text{H}_5$ transition," *Chin. Opt. Lett.* **19**(9), 091405 (2021).